

## ON THE EVIDENCE OF DISKS AROUND BLUE STRAGGLER STARS

JOHN M. PORTER

Astrophysics Research Institute, Liverpool John Moores University, Twelve Quays House, Egerton Wharf,  
Birkenhead, CH41 1LD, UK; jmp@astro.livjm.ac.uk

AND

R. H. D. TOWNSEND

Bartol Research Institute, University of Delaware, Newark, DE 19716; and Department of Physics and Astronomy,  
University College London, Gower Street, London, WC1E 6BT, UK; rhdt@bartol.udel.edu

Received 2004 September 29; accepted 2005 March 16; published 2005 March 23

### ABSTRACT

Recent observations of blue stragglers by O. De Marco et al. have revealed continuum deficits on the blue side of the Balmer discontinuity, leading these authors to infer the presence of disks around the stars. This intriguing possibility may throw light on aspects of the mechanisms responsible for at least some of these objects; current theories of blue straggler formation invoke stellar collisions or interacting binaries, both of which appear capable of forming a circumstellar disk. However, by synthesizing photospheric spectra for models of rotating blue stragglers, we demonstrate that the Balmer jump enhancements can be wholly attributed to the influence of oblateness and gravity darkening on the formation of the continuum. Therefore, we are led to conclude that the observations of De Marco et al. can be ascribed a more prosaic explanation, that of rapid stellar rotation arising from the merger/interaction formation process.

*Subject headings:* blue stragglers — stars: atmospheres — stars: rotation — techniques: spectroscopic

### 1. INTRODUCTION

Blue stragglers (BSs) are cluster stars having anomalous evolutionary histories. They are blue stars of intermediate mass (a few solar masses; Shara et al. 1997), with typical surface temperatures of  $\sim 6000$ – $10,000$  K (e.g., Deng et al. 1999). Application of single-star evolution theory indicates an age too young to be explained by the age of their parent cluster (see the review by Livio 1993 and references therein). This apparent paradox has been explained by two production paths for BSs: (1) collisions between two lower mass stars (e.g., see the simulations by Sills et al. 2001) and (2) mass transfer in moderately wide binary stars (e.g., Bellazzini et al. 2002). Both of these processes are likely to cause the remnant BS to spin up. Population studies of BSs have shown that both of these routes may be necessary to account for the observations (Davies et al. 2004).

Recently, De Marco et al. (2004, hereafter DM04) have presented *Hubble Space Telescope* (HST) observations of BS spectra and have argued that they detect the signature of a circumstellar disk around some of their targets. Disk formation is a common theme in BS generation, and hence the DM04 observations could shed light on the different evolutionary processes responsible for these objects. The evidence advanced for the presence of disks rests largely on an apparent continuum deficit (by  $\sim 5\%$ – $10\%$ ), falling on the short-wavelength side of the Balmer discontinuity; DM04 interpret this deficit—and the corresponding *enhancement* in the magnitude of the Balmer jump—as arising from circumstellar absorption by the presumed disk.

On account of their putative formation mechanisms, BSs are expected to exhibit moderate to high rotation rates. In this Letter, we investigate the effect of such rapid rotation on the photospheric continuum, by developing a spectral synthesis model that correctly accounts for the oblateness and gravity darkening arising from the centrifugal force. We describe the model in § 2 and use it in § 3 to explore the evolution of the Balmer jump as the rotation rate is varied. In § 4, we then

apply the model to the blue straggler M3-17, demonstrating that it can successfully reproduce the observations by DM04. We discuss and summarize our findings in § 5.

### 2. SPECTRAL SYNTHESIS MODEL

In a nonrotating, spherical star, the atmosphere across the entire surface may be characterized by a single value each for the effective temperature  $T_{\text{eff}}$  and gravity  $g$ . With the introduction of rotation, however, the outward pull of the centrifugal force distorts the star into an oblate spheroid. Across the surface of this spheroid, the effective gravity  $g_{\text{eff}}$  (composed of the vector sum of the Newtonian gravity and the centrifugal acceleration) is nonuniform, decreasing toward the equatorial regions where the centrifugal force is strongest. Likewise, in accordance with the gravity darkening law of von Zeipel (1924), the effective temperature decreases toward the equator in accordance with the relation  $T_{\text{eff}} \propto g_{\text{eff}}^{1/4}$ .

To model such an oblate, gravity-darkened star, we set up a raster grid that divides the surface<sup>1</sup> into about 14,000 pixels,<sup>2</sup> each covering an area  $0.015R_p$  square, where  $R_p$  is the star's polar radius. We calculate the local effective gravity associated with the surface point to which each pixel corresponds, and we likewise assign a local effective temperature

$$T_{\text{eff}} = \left( \frac{4\pi R_p^2 g_{\text{eff}}}{\Sigma_1} \right)^{1/4} T_{\text{eff},0}, \quad (1)$$

following von Zeipel's law. The overall normalization of these temperature data is specified by the notional effective temperature  $T_{\text{eff},0}$  that the star would have if it were nonrotating, under the (reasonably accurate) *Ansatz* that the stellar bolometric luminosity remains invariant as the rotation rate changes. The

<sup>1</sup> Defined by an isosurface of the effective potential within the Roche approximation (see, e.g., Cranmer 1996).

<sup>2</sup> The exact number of pixels composing the surface varies with the degree of centrifugal distortion of the star.

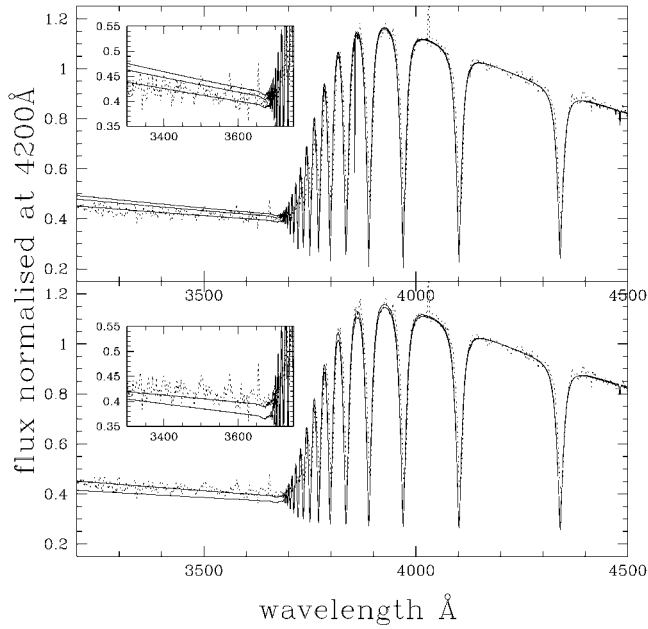


FIG. 1.—Synthetic spectra from rotating stars. The top panel shows a non-rotating model and (decreasing downward for wavelengths less than 3700 Å) models for  $v_{\text{eq}}/v_{\text{crit}} = 0.3$  and 0.5, while the bottom panel shows models for  $v_{\text{eq}}/v_{\text{crit}} = 0.7$  and 0.9 (increasing upward). All models are equator-on (inclination  $i = 90^\circ$ ). The insets are the models presented over a smaller wavelength range to highlight the flux shortward of the Balmer jump. The dotted line on all panels shows the spectrum of M3-17.

symbol  $\Sigma_1$  denotes the surface-area-weighted gravity of the distorted star, which depends among other things on the rotation rate (see eqs. [4.22]–[4.24] of Cranmer 1996).

Knowing the effective temperature and gravity of each pixel, and furthermore the local projection cosine  $\mu$  of the surface normal onto the line of sight, we interpolate the observer-directed emergent flux in a  $(T_{\text{eff}}, \log g, \mu)$ -grid of precomputed angle-dependent intensity spectra. By co-adding the flux data from all pixels, weighted by their projected area  $(0.015R_p)^2$  and Doppler shifted by the line-of-sight velocity owing to rotation, we thereby build up an integrated spectrum for the entire distorted, gravity-darkened star. For the calculations presented in § 3, we adopt an intensity spectrum grid calculated using the SYNSPEC spectral synthesis code of I. Hubeny and T. Lanz. The spectra incorporate lines due to H, He, C, N, O, Si, Mg, and Ne and are based on the “am20ak2-odfnew” grid of line-blanketed LTE model atmospheres published by Kurucz (1993; these have H/He = 0.34 by mass and are alpha enhanced by 0.4 dex and metal depleted by 2.0 dex).

### 3. INFLUENCE OF ROTATION ON THE BALMER JUMP AND COLORS

In Figure 1, we present synthetic spectra covering the wavelength range 3200–4500 Å, calculated for equatorial rotation rates  $v_{\text{eq}}/v_{\text{crit}} = 0.0, 0.3, 0.5, 0.7,$  and 0.9 using the model we describe above; here  $v_{\text{crit}} \equiv (2GM_*/3R_p)^{1/2}$  is the critical rotation velocity at which the equatorial centrifugal force balances gravity. The underlying star has a mass  $M_* = 1.35 M_\odot$ , polar radius  $R_p = 2.4 R_\odot$ , and “nonrotating” effective temperature  $T_{\text{eff},0} = 10,000$  K, these parameters being chosen to coincide with those given by DM04 for the star M3-17. The model star is viewed equator-on, and we normalize all spectra to have a unit flux at 4200 Å.

It is clear that the synthetic spectra are all similar longward

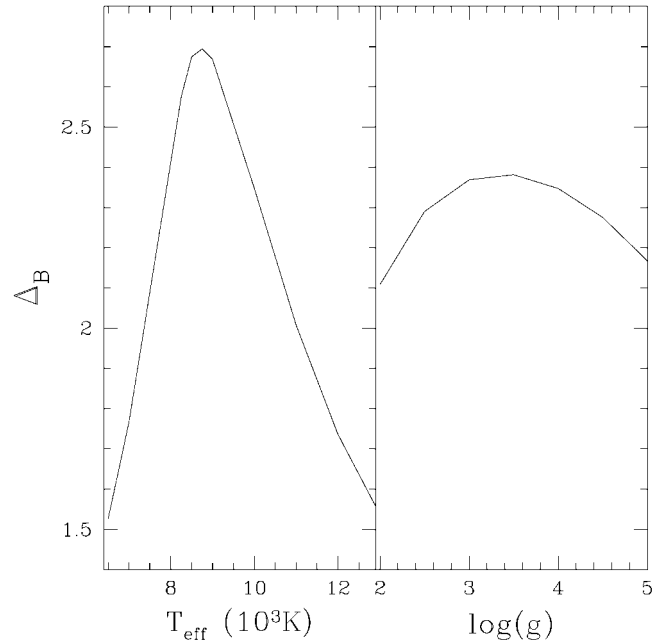


FIG. 2.—Balmer jump magnitude  $\Delta_B$  plotted as a function of effective temperature at fixed  $\log g = 4.0$  (left) and as a function of gravity at fixed  $T_{\text{eff}} = 10,000$  K (right).

of the Balmer discontinuity at 3647 Å (see below) but that the magnitude of the jump—which we characterize throughout via the ratio  $\Delta_B \equiv f_{4200}/f_{3630}$  between the continuum fluxes<sup>3</sup> at 4200 and 3630 Å—varies noticeably with the rotation rate. In interpreting this behavior, we recall that the spectrum of a rotating star is a composite, made up from contributions covering a range of effective temperatures and gravities. To illustrate the sensitivity of the Balmer jump against such variation in temperature and gravity, Figure 2 plots  $\Delta_B$  as a function of both  $T_{\text{eff}}$  and  $\log g$ , for a spectrum synthesized from a nonrotating plane-parallel atmosphere model.

The temperature dependence of  $\Delta_B$  (Fig. 2, left panel) exhibits a sharp peak around  $T_{\text{eff}} \sim 8500$  K; at temperatures cooler than this turnover, the appearance of  $\text{H}^-$  bound-free opacity—which preferentially absorbs continuum photons toward longer wavelengths in the optical and UV (see, e.g., Fig. 8.3 of Gray 1992)—tends to suppress the flux redward of the Balmer discontinuity, resulting in a reduction of  $\Delta_B$ . Likewise, at temperatures hotter than 8500 K, the progressive depopulation of the  $n = 2$  (Balmer ground state) level of neutral hydrogen removes bound-free continuum opacity blueward of the discontinuity, again resulting in a reduction of  $\Delta_B$ .

Similar behavior is exhibited in the gravity dependence of the Balmer jump (Fig. 2, right panel);  $\text{H}^-$  number densities are enhanced at high gravities, owing to the corresponding increase in electron density, while  $n = 2$  level populations are depleted at low gravities, owing to the reduction in collisional recombinations that replenish these populations. Together, these processes are responsible for the decline in  $\Delta_B$  toward both low and high  $g$ .

In Figure 3, we illustrate how the combined  $T_{\text{eff}}/\log g$  sensitivities of the Balmer-jump magnitude come together in a rotating star, by plotting  $\Delta_B$  as a function of rotation rate. We use the same stellar parameters as previously but in the present case show data for both pole- and equator-on aspects. In each,

<sup>3</sup> These points being chosen as well separated from spectral lines.

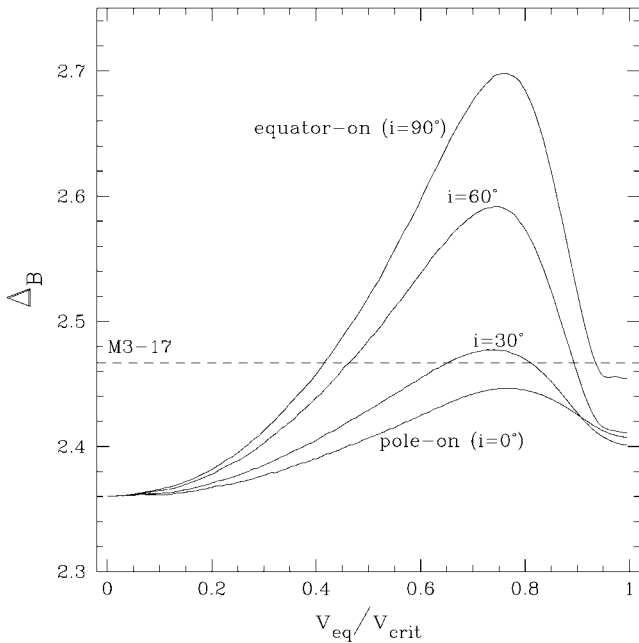


FIG. 3.—Balmer jump magnitude  $\Delta_B$  plotted as a function of rotation rate  $v_{\text{eq}}/v_{\text{crit}}$  for the stellar model representative of M3-17 (see text). Data for different inclinations are shown; the horizontal dashed line indicates the jump magnitude observed in M3-17.

$\Delta_B$  increases steadily up to a rate  $v_{\text{eq}}/v_{\text{crit}} \sim 0.77$ , owing to the reduction in equatorial effective temperature and gravity from their nonrotating values  $T_{\text{eff}} = 10,000$  K,  $\log g_{\text{eff}} = 3.81$ . At this point, the equatorial reduction of  $T_{\text{eff}}$  and  $g_{\text{eff}}$  is so pronounced that the low temperature/gravity regime of  $\Delta_B$  is reached, and the magnitude of the Balmer jump then decreases rapidly toward even higher  $v_{\text{eq}}$ . However, in every case,  $\Delta_B$  for the rotating models is larger than in the nonrotating limit.

How then does rotation change the flux distribution redward of the Balmer jump? In Figure 4, we present a color-color diagram of the rotating models. The fluxes in the three photometric bands (centered at 3660, 4200, and 5450 Å) are averaged over 120, 80, and 120 Å widths, respectively, and we use the zero-point magnitudes from Bessell et al. (1998)—this is exactly the same as the procedure used in DM04 to allow a direct comparison to be made. A grid of nonrotating model atmospheres is plotted (dotted lines) for temperatures between 8500 and 12,000 K and for  $\log g = 2.5$ –5.0. Also we have calculated pole-on and equator-on rotating atmosphere models (for  $v_{\text{eq}}/v_{\text{crit}} = 0.0$ –0.9 in steps of 0.1) for the [4200] – [5450] extreme blue edge of the nonrotating grid. The equator-on models (filled circles) sweep down and to the right (almost appearing like models becoming cooler at constant  $\log g$ ), with the lower temperature models eventually sweeping upward in a broad “U” shape. The loci of the pole-on models (filled squares) initially move vertically down with increasing rotation (i.e., no change in the [4200] – [5450] color) with the cooler models then reversing their track in a “V” shape. The maximum change in [3660] – [4200] becomes more pronounced for higher temperature models, reaching 0.06 mag for the 12,000 K model.

Two conclusions can be drawn from this figure: first, that for pole-on models, rotation can cause the Balmer jump (signified by the [3660] – [4200] color) to be too large while keeping the [4200] – [5450] color constant; second, if they are rotating, stars can exist with colors that are apparently inconsistent with nonrotating model atmospheres (i.e., the lower left-hand extremum

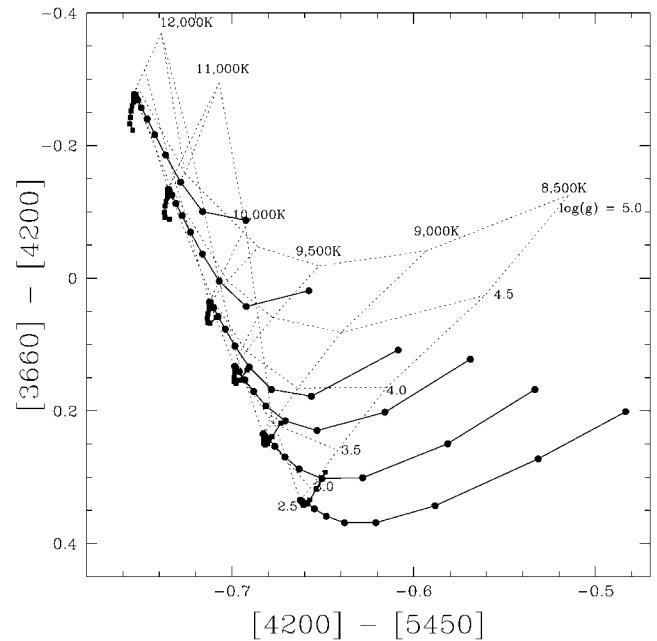


FIG. 4.—Color-color figure for both rotating and nonrotating atmosphere models. The dotted lines (with effective temperatures and gravities marked) correspond to models with zero rotation. The solid lines correspond to models with rotation rates of  $v/v_{\text{crit}} = 0.0$ –0.9 in steps of 0.1 for pole-on (squares) and equator-on (circles) models.

of the nonrotating atmosphere grid is extended a little). Finally, we note that the position of a star in the color-color plane does not yield a unique pair of effective temperature and gravity values—two color measurements cannot produce three unique values of effective temperature, gravity, and rotation.

#### 4. APPLICATION TO M3-17

The observed projected rotation velocity of M3-17,  $v \sin i = 200 \pm 50$  km s<sup>-1</sup>, along with the stellar parameters furnished by DM04, implies that this object is a rapid rotator, having  $v_{\text{eq}} \sin i/v_{\text{crit}} = 0.75 \pm 0.18$ . The Balmer jump magnitude derived from the *HST* spectrum of this object is  $\Delta_B = 2.47$ , a value that we indicate in Figure 3 by the horizontal dashed line. Clearly, there are multiple rotating models that can fit the observations, without the need to invoke a circumstellar disk; for example, a match to  $\Delta_B$  can be achieved with an edge-on ( $i = 90^\circ$ ) model rotating at  $v_{\text{eq}}/v_{\text{crit}} \approx 0.4$  or 0.9, and other solutions can be found at lesser inclinations.

We further illustrate this point in Figure 1, where we plot the archival spectrum of M3-17 over our model data. The nonrotating synthetic spectrum clearly has a surfeit of continuum flux shortward of the Balmer discontinuity, which led DM04 to diagnose the presence of a circumstellar disk. However, our equator-on rotating models at  $v_{\text{eq}}/v_{\text{crit}} = 0.4$  and 0.9 clearly provide a good fit to the continuum flux, suggesting that rotation alone may suffice to explain the Balmer jump. In support of this conclusion, we note that the rotational reddening of the Paschen continuum, as seen for the equator-on curves in Figure 4, actually enables the rotating models to fit the observed [4200] – [5450] color of M3-17 better than the nonrotating model of the same temperature. We do observe that our models are unable to reproduce the strengths of the Balmer series absorption lines seen redward of 3647 Å; this problem reflects the fact that we specify the model temperature a priori from that of DM04. The issue can be resolved by allowing  $T_{\text{eff},0}$  (and other parameters) to vary

under the control of a suitably chosen fitting statistic. However, we do not undertake such fine-tuning here, because we are not attempting to derive exact atmospheric parameters for M3-17 here. Rather, our objective is to highlight that high rotation has a significant effect on the continuum and may mimic the presence of an obscuring disk.

#### 5. DISCUSSION AND SUMMARY

Using a spectral synthesis approach that correctly treats oblateness and gravity darkening, we have demonstrated that apparent flux deficits shortward of the Balmer discontinuity can be attributed wholly to rapid rotation. This casts doubt on the disk hypothesis advanced by DM04 to explain the Balmer jump anomalies seen in the spectra of BSs. At least in the case of rapid rotator M3-17 ( $v \sin i = 200 \pm 50 \text{ km s}^{-1}$ ), the continuum is well fit by our model, leaving little reason to invoke the presence of a disk.

In addition to M3-17, five other stars (out of a total of 50) in the DM04 sample show Balmer jumps that are enhanced with respect to nonrotating models.<sup>4</sup> Of these five, only NGC

<sup>4</sup> By this, we mean models that do not include oblateness or gravity darkening.

6751-11 has a measured (upper limit) projected rotation velocity,  $v \sin i < 50 \text{ km s}^{-1}$ . Because of the unknown projection factor  $\sin i$ , the upper limit on the intrinsic equatorial velocity  $v_{\text{eq}}$  may be much larger, and it is entirely possible that, along with the remaining objects with anomalous Balmer jumps, this star is a rapid rotator.

Accordingly, Balmer jump anomalies seen in BSs may *all* be attributable to rapid rotation. This hypothesis is lent some support by the fact that the proposed formation mechanisms for BSs—collisions or mass transfer—both involve the deposition of significant amounts of angular momentum on the star, thereby spinning it up (see, e.g., Pols & Marinus 1994).

On a final note, we stress that we do not (and cannot) rule out the possibility of disks around BSs. Indeed, observations of emission lines in these objects, bearing a close resemblance to those seen in Be stars (see Mermilliod 1982), indicate that there almost certainly *are* circumstellar disks around some of them. However, the present Letter demonstrates why Balmer jump anomalies cannot be used as a clear and unambiguous diagnostic for BS disks.

R. H. D. T. acknowledges support from PPARC and from NSF grant AST-0097983. We thank the referee for his/her useful comments on the submitted Letter.

#### REFERENCES

- Bellazzini, M., Fusi Pecci, F., Messineo, M., Monaco, L., & Rood, R. T. 2002, *AJ*, 123, 1509
- Bessell, M. S., Castelli, F., & Plez, B. 1998, *A&A*, 333, 231
- Cranmer, S. R. 1996, Ph.D. thesis, Univ. Delaware
- Davies, M. B., Piotto, G., & de Angeli, F. 2004, *MNRAS*, 349, 129
- De Marco, O., Lanz, T., Ouellette, J. A., Zurek, D., & Shara, M. M. 2004, *ApJ*, 606, L151 (DM04)
- Deng, L., Chen, R., Liu, X. S., & Chen, J. S. 1999, *ApJ*, 524, 824
- Gray, D. F. 1992, *The Observation and Analysis of Stellar Photospheres* (2nd ed.; Cambridge: Cambridge Univ. Press)
- Kurucz, R. L. 1993, CD-ROM 16, Limbdarkening for 2 km/s Grid (No. 13): [+1.0] to [-1.0] (Cambridge: SAO)
- Livio, M. 1993, in *ASP Conf. Ser. 53, Blue Stragglers*, ed. R. A. Staffer (San Francisco: ASP), 3
- Mermilliod, J.-C. 1982, *A&A*, 109, 37
- Pols, O. R., & Marinus, M. 1994, *A&A*, 288, 475
- Shara, M. M., Saffer, R. A., & Livio, M. 1997, *ApJ*, 489, L59
- Sills, A., Faber, J. A., Lombardi, J. C., Rasio, F. A., & Warren, A. R. 2001, *ApJ*, 548, 323
- von Zeipel, H. 1924, *MNRAS*, 84, 665